INAF
ISTITUTO NAZIONALE
DI ASTROFISICA
NATIONAL INSTITUTE
FOR ASTROPHYSICS

Publication Year	2024
Acceptance in OA	2025-01-21T11:30:11Z
Title	The curious case of 2MASS J15594729+4403595, an ultra-fast M2 dwarf with possible Rieger cycles
Authors	MESSINA, Sergio, CATANZARO, Giovanni, LANZA, Antonino Francesco, Gandolfi, D., Serrano, M. M., Deeg, H. J., García-Alvarez, D.
Publisher's version (DOI)	10.1051/0004-6361/202449959
Handle	http://hdl.handle.net/20.500.12386/35674
Journal	ASTRONOMY & ASTROPHYSICS
Volume	691

7. Discussion

The RV variability unveiled by our measurements complemented with the ones from the literature and the large RUWE value of about 13 reported in the *Gaia* DR3 allow us to state that the primary component of 2MASS J15594729+4403595 is a close binary and, since no evidence of spectral features of its secondary have been detected in our high-resolution spectra, we can classify it as an SB1 system. This means that 2MASS J15594729+4403595 is a hierarchical triple system, consisting of an unresolved M2+? close binary and a visual M8 component. Unfortunately, neither TESS nor Zeta UMa observations could spatially resolve the two components of the SB1 system or the primary M1 from the secondary M8 component, their spatial resolutions being 21″/pixel and 1.5″/pixel, respectively. Since 2MASS J15594729+4403595 is a photometrically unresolved system in our study, the analysed photometry contains signals from all three components. However, the M8 component is about six magnitudes fainter than the primary in the i' band, which implies that its flux contribution is about a factor of 250 smaller than that of the primary. Therefore, its contribution to the observed variability is negligible. Since the secondary unseen component of the SB1 is expected to be much fainter than the primary, as our spectroscopic analysis indicates, its contribution to the total flux is also expected to be negligible. In this circumstance, the observed photometric variability is dominated by the primary component.

If this is the correct scenario, we deal with a star with a rotation period of $P_1 = 0.3700$ d and spots on opposite hemispheres that produce a secondary rotational modulation with a period given by the first harmonic ($P_3 = 0.1850$ d).

Interpreting the presence of the periodicity, $P_2 = 0.44298$ d, is challenging. In this context, it is relevant to remind ourselves that the P_2 periodicity clearly detected during TESS observations was not detected in the data time series collected at the Zeta UMa Observatory in 2014, although that photometry was precise enough to detect it, if it were present. In this respect, it will be very interesting to check if P_2 is also absent in the *Gaia* time series that was collected almost contemporaneously, but that has not yet been released. In what follows, we present different possible interpretations for the existence of the $P_2 = 0.44298$ d periodicity.

7.1. Ellipsoidicity

A first hypothesis to account for the P_2 periodicity is that the primary component has the secondary so close as to suffer from some level of ellipsoidal tidal deformation. In such a case, the changing projected surface of the primary can produce a rotational modulation with the SB1 orbital period of $P_2 = 0.4429$ d. In this case, we were dealing with an un-synchronised system for which the axial rotation period, P_1, is smaller than the tentatively estimated orbital period, P_2. However, our periodogram analysis of the RV time series does not show any significant power peak at such a period, whereas the best orbital solution has an orbital period of about 14 days. Moreover, in this hypothesis, the periodicity should be permanent, whereas, as was mentioned, it was not detected in the data of the 2013 photometric campaign. We could consider also the case of a star that is precessing without having a disc. The precession would be caused by a misalignment between the stellar equator and the orbital plane, which could be possible, given that the star is relatively young. Nevertheless, this model implies that the periodicity is permanent, which is not in agreement with the observations. Moreover, we would expect a precession period longer than the orbital period; that is, longer than 14 days. Were the *Gaia* photometry to confirm that P_2 was not present, we could exclude the ellipsoidicity hypothesis and consider the following hypotheses.

7.2. Clumpy disc

Another possible interpretation to account for the P_2 periodicity is that 2MASS J15594729+4403595 has a disc with some sort of clumpy structure that, when the precession allows the disc to pass in front of the star, periodically transits across the stellar disc (see, e.g. Rodríguez-Ledesma et al. 2012) and produces the observed rotational modulation with a keplerian period, P_2, longer than the stellar rotation period, P_1. However, the estimated age does not fit well with the presence of a dusty disc (e.g. Ribas et al. 2015), unless it is a debris disc.

7.3. Surface differential rotation

Another possible interpretation is in terms of SDR. In fact, on a differentially rotating star, spots at different latitudes can produce rotational modulations of different periods. If this is the case, the relative rotation period difference, $(P_2 - P_1)/P_2$, would imply an SDR amplitude of about 16%. According to Küker et al. (2019), such a star should have a differential rotation not larger than a few percent owing to its very fast rotation. Very fast rotators are expected to behave as rigid bodies. In a sample of over 18 000 Kepler stars with measured SDR, Reinhold et al. (2013) found the relative shear, $\Delta\Omega/\Omega$, to decrease with a decreasing rotation period, and to further slightly decrease with effective temperature. On the other hand, according to the simulations by Brun et al. (2022), this large value is not unlikely. Depending on the latitudes at which major spot centres are located, differential rotation may not be detectable, as it happened in the 2013 observations.

7.4. Rossby waves and Rieger cycles

We considered the frequency, $\sigma_{\rm obs}$, of a Rossby wave seen by a distant observer,

$$\sigma_{\rm obs} = m\Omega + \sigma, \tag{4}$$

with the frequency of the wave in a reference frame rotating with the star given by

$$\sigma = -\frac{2m\Omega}{n(n+1)}, \tag{5}$$

where the minus sign comes from the retrograde propagation of the wave in the rotating frame, m is the azimuthal wavenumber, $\Omega \equiv 2\pi/P_{\rm rot}$ the stellar rotation frequency, and n the degree of the wave (see Zaqarashvili et al. 2021, Eq. 30 for details). The transformation of the frequency from the reference frame rotating with the star to that of a distant observer is discussed in, for example, Kepler (1984) and Unno et al. (1989). In principle, the effects of the rapid rotation and strong magnetic fields on the eigenfrequencies of the Rossby waves cannot be neglected. An analysis is presented in Appendix C, in which we show that the centrifugal deformation of the star has a negligible effect, provided that the wave is propagating close to the interface between the convection zone and the radiative interior, while strong magnetic fields can be neglected because the Coriolis force is much stronger than the Lorentz force in our rapidly rotating star.

In the specific case of the active component of 2MASS J15594729+4403595, we adopted $n = 3, m = 1$, which give a periodicity in the observer's frame of $(6/5)P_{\rm rot} = 0.444$ d, when a rotation period, $P_{\rm rot} = P_1 = 0.370$ d, is adopted. Rossby waves are waves of vorticity; therefore, they do not directly produce brightness oscillations as in the case, for example, of p-mode waves, which produce temperature and density perturbations. Nevertheless, considering that those waves can affect the emergence and the distribution of magnetic structures – for example, in the solar corona (cf. Sect. 4.2 of Zaqarashvili et al. 2021) – it is not excluded that they can produce brightness oscillations in our very active star, thereby accounting for the P_2 periodicity as seen by a distant observer. On the other hand, a modulation of the magnetic flux emergence possibly associated with the same Rossby wave has a period of $2\pi/\sigma = 2.25$ d in the reference frame rotating with the star. Such a modulation can induce a short-term activity cycle akin to a solar Rieger cycle in our star, as is discussed by Zaqarashvili et al. (2021) in their Sects. 4.2.4–4.2.6.

To further discriminate between the SDR and the Rieger cycle hypotheses, the spot model comes into help. As part of Test 1 in Appendix B, we built one synthetic light curve, as was produced in the case of SDR, with two active regions rotating with P_1 and P_2 periods, and ran our code to produce the corresponding map time series. Consistently with the proposed scenario, we find the total spot area (summed over all longitudes) to stay constant during consecutive rotation cycles. Similarly, as part of Test 2, we built one synthetic light curve, as was produced in the case of a cyclic modulation of the spot area induced by a Rossby wave with a period of $P = 2.25$ d in the stellar frame. We also added the brightness change produced by the wave as well as the rotational modulation of the visibility of the active regions on the stellar surface as they are seen by a distant observer. A comparison between the SDR-case and Rieger-case spot maps with those retrieved from the observed TESS time series indicates the Rieger cycle hypothesis to be the more likely one.

In our maps based on the TESS time series, we found clear evidence of a periodic variation in the spotted area, on opposite hemispheres and in the anti-phase. The timescale of the spot area variation is very short, with a period of about six stellar rotations, and its pattern has remained very stable during the three TESS sectors, spanning a time interval of about two years.

On the Sun, the lifetime of spots depends on the spot area according to the Gnevyshev–Waldmeier (GW) relation (Gnevyshev 1938). However, studies extended to solar-type stars found shorter timescales for the spot evolution compared to the solar case. From the Kepler data time series analysis, the lifetime of starspots is found in a range from 10 days to one year (e.g., Giles et al. 2017). Despite the difference in timescale, the physical mechanism, which after the magnetic field emersion into the photosphere leads to its diffusion, is probably the same.

The modulation shown by the spots on 2MASS J15594729+4403595, which is periodic ($P = 2.25$ d corresponding to six rotations), is too short to be interpreted as an active region growth and decay. In fact, this short timescale is at odds with the year-long timescale expected for the magnetic field diffusion. Rather, the change in the total spotted area observed in subsequent TESS sectors may more likely come from a modulation induced by the short-period Rossby wave, although the detailed mechanism remains elusive. In other words, the periodic oscillation that we observe in the maps in Figs. 7 and 8 may be a manifestation of a Rossby wave, more commonly referred to as r-mode or Rieger-like cycles. We notice that Rossby waves propagate in a retrograde sense in the reference frame rotating with the star, while our spot pattern is fixed in the reference frame rotating with the $P_1 = P_{\rm rot} = 0.37$ d rotation period. Nevertheless, we have assumed that the wave is propagating in the deep stellar interior; thus, it is conceivable that we can see its effects on the total spotted area without any clearly induced systematic migration of the spots in longitude at the stellar surface. Future studies could account for such a behaviour by clarifying the mechanism through which the wave affects the spot formation and location on the stellar surface. For example, the spot locations could be associated with convectively induced active longitudes that are fixed in the stellar reference frame (cf. Weber et al. 2013), while the passage of a retrograde propagating Rossby wave only induces a modulation of their levels of activity.

To put our suggestion in context, Rieger cycles have been observed in the Sun, and only recently in solar-type stars; notably, in CoRoT-2, which is a G7 dwarf with a period of $P \sim 29$ d (which corresponds to about six stellar rotations), by Lanza et al. (2009), or on Kepler-17 by Bonomo & Lanza (2012), where the cycle lasts about three stellar rotations ($P_{\rm rot} = 12$ d).

What makes 2MASS J15594729+4403595 interesting is the extremely short timescale of the candidate Rieger cycle, which is more likely related to Rossby waves than to active region growth and decay or to cyclical activity. An important characteristic of Rieger cycles is that they are not persistent, but appear close to the maxima of the solar 11-yr cycle. Also, Rossby waves have a limited lifetime in the Sun that does not exceed ∼1.4 years (Zaqarashvili et al. 2021, Sect. 4.2.2). Similarly, a limited lifetime for the Rossby waves in 2MASS J15594729+4403595 could account for the absence of the P_2 periodicity in the Zeta UMa Observatory time series.

As is shown in Fig. 4, the photometric modulation pattern shown by 2MASS J15594729+4403595 is easily recognisable. This offers a criterion to select other stars with similar patterns to be examined in search for Rieger-like cycles, and thus improves the total number and the statistics of this phenomenon on stars other than the Sun.

8. Conclusion

Our analysis has allowed us to better characterise 2MASS J15594729+4403595, which is a candidate member of the AB Dor association. Our photometric and spectroscopic observations reveal that this is a triple system consisting of a primary M2 component, which is itself a SB1 close binary, and a secondary M8 component. We have derived tentative orbital parameters that may indicate a system in an eccentric orbit with an orbital period of about 14 d. We have measured the rotation period, $P = 0.3701$ d, of the primary M2 component and inferred an inclination, $i \simeq 50°$, of the stellar spin axis to the line of sight. Another periodicity of 0.44 d could be associated with SDR or, more likely, with a Rossby wave. The spot modelling has allowed us to discover a spotted area modulation that resembles a possible Rieger-like cycle, but on a very short timescale that can be accounted for by the same Rossby wave assumed to produce the 0.44 d periodicity in the light modulation. The extremely short candidate Rieger cycle and the multiple photometric periodicities observed in 2MASS J15594729+4403595 all make this star a very interesting target for additional studies. As a future perspective, we intend to extend our analysis to other stars showing similar photometric modulation patterns to explore the presence of similar Rieger cycles.

Data availability

The ground-based photometry and the reduced spectra are available at the CDS via anonymous ftp to cdsarc.cds.unistra.fr (130.79.128.5) or via https://cdsarc.cds.unistra.fr/viz-bin/cat/J/A+A/691/A117

Acknowledgements. SM thanks Roi Alonso and Antonio Luis Cabrera Lavers for their contribution on the observational side. This research was funded by the "European Union – NextGenerationEU" RRF M4C2 1.1 n: 2022HY2NSX. "CHRONOS: adjusting the clock(s) to unveil the CHRONO-chemo-dynamical Structure of the Galaxy" (PI: S. Cassisi) and supported by the program "Stellar activity and dynamo theory in the era of precision stellar astrophysics" (PI: A. Bonanno) within Ricerca Fontamentale at INAF. Based on observations made with the Nordic Optical Telescope, owned in collaboration by the University of Turku and Aarhus University, and operated jointly by Aarhus University, the University of Turku and the University of Oslo, representing Denmark, Finland and Norway, the University of Iceland and Stockholm University at the Observatorio del Roque de los Muchachos, La Palma, Spain, of the Instituto de Astrofisica de Canarias. The TESS data presented in this paper were obtained from the Mikulski Archive for Space Telescopes (MAST). STScI is operated by the Association of Universities for Research in Astronomy, Inc., under NASA contract NAS5-26555. Support for MAST for non-HST data is provided by the NASA Office of Space Science via grant NNX13AC07G and by other grants and contracts. This research has made use of the SIMBAD database, operated at CDS, Strasbourg, France.

References

Baraffe, I., Homeier, D., Allard, F., & Chabrier, G. 2015, A&A, 577, A42
Barnes, S. A. 2003, ApJ, 586, 464
Barnes, S. A. 2007, ApJ, 669, 1167
Binks, A. S., & Jeffries, R. D. 2016, MNRAS, 455, 3345
Bonomo, A. S., & Lanza, A. F. 2012, A&A, 547, A37
Bowler, B. P., Liu, M. C., Shkolnik, E. L., & Tamura, M. 2015, ApJS, 216, 7
Brun, A. S., Strugarek, A., Noraz, Q., et al. 2022, ApJ, 926, 21
Claret, A., Hauschildt, P. H., & Witte, S. 2012, A&A, 546, A14
Drilling, J. S., & Landolt, A. U. 2000, in Allen's Astrophysical Quantities, ed. A. N. Cox, 381
Frandsen, S., & Lindberg, B. 1999, in Astrophysics with the NOT, eds. H. Karttunen, & V. Piirola, 71
Gallet, F., & Bouvier, J. 2013, A&A, 556, A36
Gandolfi, D., Parviainen, H., Fridlund, M., et al. 2013, A&A, 557, A74
Giles, H. A. C., Collier Cameron, A., & Haywood, R. D. 2017, MNRAS, 472, 1618
Głębocki, R., & Gnaciński, P. 2005, ESA Spec. Publ., 560, 571
Gnevyshev, M. N. 1938, Izvestiya Glavnoj Astronomicheskoj Observatorii v Pulkove, 16, 36
Herbst, W., Bailer-Jones, C. A. L., Mundt, R., Meisenheimer, K., & Wackermann, R. 2002, A&A, 396, 513
Janson, M., Hormuth, F., Bergfors, C., et al. 2012, ApJ, 754, 44
Jönsson, H., Holtzman, J. A., Allende Prieto, C., et al. 2020, AJ, 160, 120
Kepler, S. O. 1984, ApJ, 286, 314
Koenigl, A. 1991, ApJ, 370, L39
Küker, M., Rüdiger, G., Olah, K., & Strassmeier, K. G. 2019, A&A, 622, A40
Lamm, M. H., Bailer-Jones, C. A. L., Mundt, R., Herbst, W., & Scholz, A. 2004, A&A, 417, 557
Lanza, A. F. 2016, Lect. Notes Phys., 914, 43
Lanza, A. F., Catalano, S., Cutispoto, G., Pagano, I., & Rodono, M. 1998, A&A, 332, 541
Lanza, A. F., Pagano, I., Leto, G., et al. 2009, A&A, 493, 193
Lépine, S., Hilton, E. J., Mann, A. W., et al. 2013, AJ, 145, 102
Malo, L., Artigau, É., Doyon, R., et al. 2014, ApJ, 788, 81
Matt, S. P., Brun, A. S., Baraffe, I., Bouvier, J., & Chabrier, G. 2015, ApJ, 799, L23
Messina, S. 2008, A&A, 480, 495
Messina, S. 2019, A&A, 627, A97
Messina, S., Desidera, S., Turatto, M., Lanzafame, A. C., & Guinan, E. F. 2010, A&A, 520, A15
Messina, S., Desidera, S., Lanzafame, A. C., Turatto, M., & Guinan, E. F. 2011, A&A, 532, A10
Messina, S., Lanzafame, A. C., Malo, L., et al. 2017a, A&A, 607, A3
Messina, S., Millward, M., Buccino, A., et al. 2017b, A&A, 600, A83
Paxton, B., Smolec, R., Schwab, J., et al. 2019, ApJS, 243, 10
Pecaut, M. J., & Mamajek, E. E. 2013, ApJS, 208, 9
Provost, J., Berthomieu, G., & Rocca, A. 1981, A&A, 94, 126
Reinhold, T., Reiners, A., & Basri, G. 2013, A&A, 560, A4
Riaz, B., Gizis, J. E., & Harvin, J. 2006, AJ, 132, 866
Ribas, Á., Bouy, H., & Merín, B. 2015, A&A, 576, A52
Roberts, D. H., Lehar, J., & Dreher, J. W. 1987, AJ, 93, 968
Rodríguez-Ledesma, M. V., Mundt, R., Ibrahimov, M., et al. 2012, A&A, 544, A112
Shu, F., Najita, J., Ostriker, E., et al. 1994, ApJ, 429, 781
Silva-Beyer, J., Godoy-Rivera, D., Chanamé, J., et al. 2022, ArXiv e-prints [arXiv:2210.01137]
Telting, J. H., Avila, G., Buchhave, L., et al. 2014, Astron. Nachr., 335, 41
Unno, W., Osaki, Y., Ando, H., Saio, H., & Shibahashi, H. 1989, Nonradial Oscillations of Stars (Tokyo: University of Tokyo Press)
Voges, W., Aschenbach, B., Boller, T., et al. 1999, A&A, 349, 389
Weber, M. A., Fan, Y., & Miesch, M. S. 2013, ApJ, 770, 149
Zacharias, N., Monet, D. G., Levine, S. E., et al. 2005, VizieR Online Data Catalog: I/297
Zaqarashvili, T. V., Albekioni, M., Ballester, J. L., et al. 2021, Space Sci. Rev., 217, 15
Zechmeister, M., & Kürster, M. 2009, A&A, 496, 577
Zickgraf, F. J., Engels, D., Hagen, H. J., Reimers, D., & Voges, W. 2003, A&A, 406, 535

Appendix A: Zeta UMa Observatory photometry

To determine the stellar rotation period, we carried out a multi-band photometric monitoring in 2013 at the Zeta UMa Observatory (709 m a.s.l.; Madrid, Spain).

The observations were collected by a 130mm Takahashi refractor equipped with a cooled QHY9 camera and a set of V and R Johnson-Cousins filters. The telescope field of view (FoV) of about $80' \times 60'$ was centred on our target star. The observations were carried out for a total of 12 nights from May 31 to August 08, 2013. We collected a total of 2355 frames in the V and 120 in the R filter (see Table A2). The integration of 100 s on the first night was reduced to 50 s on subsequent nights owing to saturation of the brightest stars in the FoV. On each clear night, our target was observed continuously for about 5-6 hr together with a series of bias and flat-field frames.

The data reduction was carried out using the DAOPHOT tasks within IRAF[2]. After bias subtraction and flat-fielding, we extracted the magnitudes of all stars detected in each frame using a set of different apertures. We selected the aperture giving the best photometric accuracy of our target and comparison stars. After removing outliers by applying a 3σ threshold, we were left with 2251 V-band and 112 R-band measurements useful for the subsequent analysis. We identified three stars close to the FoV centre and non-variable during the whole period of our observations which served as comparison (C) and check (CK) stars to get differential magnitudes of our target (see Table A.1). The nominal accuracy of our observations is better than 0.005 mag in the magnitude range of our target and comparison stars. However, to measure the effective photometric accuracy of our observations, instead of using the values provided by DAOPHOT and based on photon statistics, we sectioned our time series into bins of 15 minutes width (corresponding on average to 8-9 consecutive measurements) computing means and standard deviations. We found that the average standard deviation for the binned V−C measurements was $\sigma_{V-C} = 0.006$ mag, whereas $\sigma_{CK1-C} \simeq \sigma_{CK2-C} = 0.010$ mag. These values represent a more effective estimate of the precision of our photometry (see Table A.1 for the precision in the whole time series).

Appendix B: Spot Model

B.1. Code description

We apply a spot modelling approach already introduced in Sect. 3 of Bonomo & Lanza (2012) to which we refer the reader for details. Briefly, the surface of the star is subdivided into 200 surface elements that contain unperturbed photosphere and dark spots. The specific intensity of the unperturbed photosphere in the TESS passband is assumed to vary according to a quadratic limb-darkening law:

$$I(\mu) = I_0(a_p + b_p\mu + c_p\mu^2) \tag{B.1}$$

where I_0 is the specific intensity at the centre of the disc, $\mu = \cos\theta$ with θ being the angle between the local surface normal and the line of sight, and a_p, b_p, and c_p are the limb-darkening coefficients in the TESS passband. The dark spots are assumed to have a fixed contrast $c_s = I_{spot}(\mu)/I(\mu)$ in the TESS passband, where I_{spot} is the specific intensity in the spotted photosphere. The fraction of a surface element covered by dark spots is given by its filling factor f.

This model is fitted to a segment of the light curve of duration Δt_f, which is set equal to one stellar rotation period, by varying the filling factors of the individual surface elements that can be represented as a 200-element vector $\boldsymbol{f}$. Therefore, the model has 200 free parameters and suffers from non-uniqueness and instability due to the effect of photometric noise. To select a unique and stable solution, we apply a maximum entropy (ME) regularisation by minimising a functional Z that is a linear combination of the χ^2 and of a suitable entropy function S:

$$Z = \chi^2(\boldsymbol{f}) - \lambda S(\boldsymbol{f}), \tag{B.2}$$

where $\lambda > 0$ is a Lagrangian multiplier that controls the relative weights given to the χ^2 minimisation and to the configuration entropy of the surface map S in the solution. The expression of S is given in Eq. (5) of Bonomo & Lanza (2012); it is maximal when the star is unspotted, that is, when all the elements of the vector $\boldsymbol{f}$ are zero. In other words, the ME criterion selects the solution with the minimum spotted area compatible with a given χ^2 value of the best fit to the light curve. When the Lagrangian multiplier $\lambda = 0$, we obtain the solution corresponding to the minimum χ^2 that is unstable. By increasing λ, we obtain a unique and stable solution at the price of increasing the value of the χ^2. An additional effect is that of making the residuals between the model and the light curve biased towards negative values because we reduce the spot filling factors by introducing the entropy term (see Lanza et al. 1998; Lanza 2016 for details). The information on the latitude of the spots is lacking in our maximum-entropy maps although the inclination of the stellar spin axis $i = 50$ deg is far from being equator-on. Therefore, we limit ourselves to mapping the distribution of the filling factor versus the longitude.

The optimal value of the Lagrangian multiplier λ is obtained by imposing that the mean $|\mu_{reg}|$ of the residuals between the regularised model and the light curve verifies the relationship (Bonomo & Lanza 2012; Lanza 2016):

$$|\mu_{reg}| = \sigma_0 / \sqrt{N} \tag{B.3}$$

where σ_0 is the standard deviation of the residuals of the unregularised model, that is, that computed with $\lambda = 0$, with N being the number of datapoints in the fitted light curve interval of duration Δt_f.

B.2. Testing spot modelling results

The spot pattern presented in Sect. 6 may be in principle an artifact of the code, arising from its attempt to model the beat-like pattern of the observed light curve. To explore this possibility, as well as to discriminate between the SDR and Rossby wave interpretations presented in Sect. 7, we performed two tests by using synthetic light curves.

Test 1 - Surface differential rotation.
We have combined two different synthetic sinusoids which represent the flux rotational modulations with the two periods $P_1 = 0.37$ d (the rotation period of the major spot group) and $P_2 = 0.443$ d (the rotation period of the secondary spot group at a different latitude). The amplitudes of the photometric modulations are similar to those observed and a level of Gaussian noise comparable to the observed one was added:

$$flux = A_1 + B_1\cos(\omega_1 t) + A_2 + B_2\cos(\omega_2 t) + \epsilon, \tag{B.4}$$

where $\omega_1 = 2\pi/P_1$ and $\omega_2 = 2\pi/P_2$, t is the time, and ϵ a white Gaussian noise.

[2] IRAF is distributed by the National Optical Astronomy Observatory, which is operated by the Association of the Universities for Research in Astronomy, inc. (AURA) under cooperative agreement with the National Science Foundation.

Table A.1. List of targets for differential photometry.

	Name	RA (J2000.)	DEC (J2000.)	Vmag (mag)	$\sigma_{\star-c}$ (mag)
V	2MASS J15594729+4403595	15:59:47.29	+44:03:59.5	11.86	0.008
C	TYC 3067-1461-1	16:00:01.86	+44:06:01.8	11.37	...
CK1	TYC 3060-1156-1	15 59 42.27	+43:59:17.2	11.00	0.012
CK2	2MASS J15595409+4358586	15:59:54.10	+43:58:58.8	12.57	0.015

Notes. Target (V), comparison (C), and check stars (CK) used for the differential photometry.

Table A2. Log of observations at the Zeta UMa Observatory.

Date	HJD_{mean}	# Frame V-band	# Frame R-band
2013-05-31	2456444.49770	149	12
2013-06-01	2456445.52872	274	12
2013-06-14	2456458.49934	219	12
2013-06-15	2456459.51744	270	12
2013-06-22	2456466.46756	45	12
2013-06-28	2456472.53530	253	12
2013-06-29	2456473.49245	177	12
2013-07-26	2456500.42421	140	12
2013-07-30	2456504.45789	203	12
2013-08-02	2456507.47174	223	12
2013-08-03	2456508.42086	166	...
2013-08-08	2456513.44935	236	...

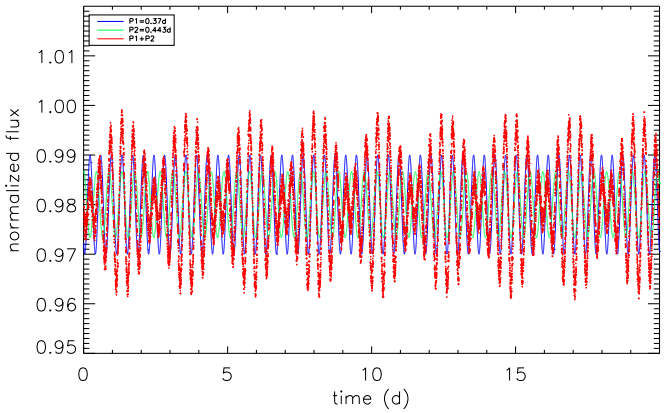

Fig. B.1. Synthetic light curve (red) obtained combining two sinusoids with $P_1 = 0.37$ d (blue line) and $P_2 = 0.443$ d (green line) in the Test 1 (Surface differential rotation).

We got the synthetic light curve shown in Fig. B.1. Then, we run our spot model on this light curve and obtained the spot map shown in Fig. B.2.

We find the activity mostly located on one longitude only with a clear drift toward decreasing longitudes with a periodicity equal to the 2.25-d beating period and with the total spotted area to remain constant from cycle to cycle.

Test 2 - Rieger cycle.

We have generated a synthetic light curve which is a sinusoid with period $P_1 = 0.37$ d (the stellar rotation period) whose amplitude is modulated by another sinusoid with a period $P_2 = 2.25$ d, mimicking some sort of a cycle in the spottedness level. We also add the rotation period first harmonic $P_3 = 0.1849$ d and

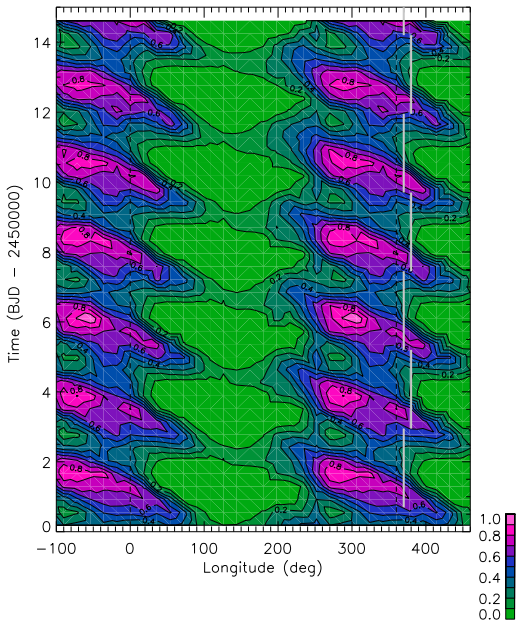

Fig. B.2. Maps time series retrieved by modelling the synthetic light curve in Fig. B.1.

the $P_4 = 0.443$ d periodicity. A Gaussian noise comparable to the observed one was added to the synthetic data and the sinusoid amplitudes were chosen to reproduce the observed ones. Specifically, we simulate the effect of the spot area modulation with the period P_2 as

$$flux = A(t)\sin(\omega_1 t) \tag{B.5}$$

where

$$A(t) = A_0 + B_0\cos(\omega_2 t). \tag{B.6}$$

To such a flux modulation we add the effects of the rotation and of the Rossby wave as seen by a distant observer with periods P_1 and P_4, respectively. Using the Werner formula, the total flux f can be written as

$$f = A_0\sin(\omega_1 t) + \frac{1}{2}B_0\{\sin[(\omega_1+\omega_2)t] + \sin[(\omega_1-\omega_2)t]\} + A_3\sin(\omega_3 t) + A_4\sin(\omega_4 t) + \epsilon \tag{B.7}$$

where $\omega_1 = 2\pi/P_1$, $\omega_2 = 2\pi/P_2$, $\omega_3 = 2\pi/P_3$, $\omega_4 = 2\pi/P_4$, t is the time, and ϵ a white Gaussian noise. We get the synthetic light curve shown in Fig. B.3. We modelled this light curve and obtained the spot pattern shown in Fig. B.4.

If we compare the results of our Test 1 and 2 with the maps obtained from the observed data, Test 2 seems to better explain

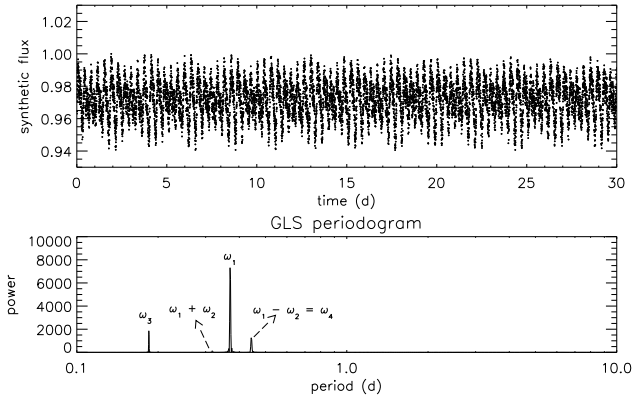

Fig. B.3. Periodogram analysis for Test 2 light curve. Top panel: Synthetic light curve for the Test 2. Bottom panels: the GLS periodogram where the main frequencies as detected in the observed time series are all retrieved. The level corresponding to the white Gaussian noise added to take into account the photon shot noise is very low and does not appear in the periodogram.

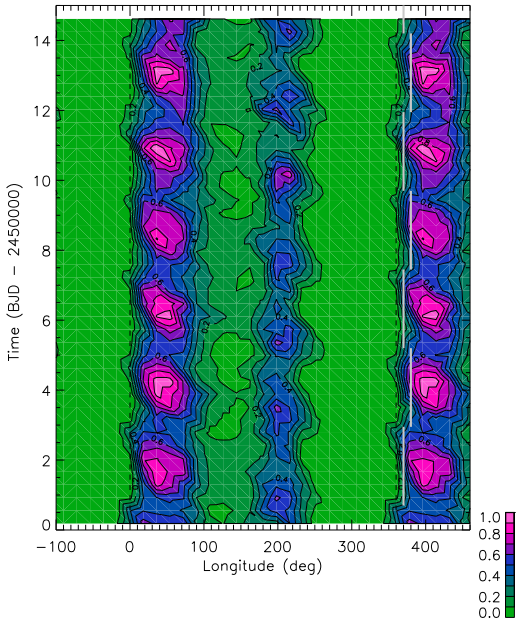

Fig. B.4. Map time series retrieved by modelling the synthetic light curve in Fig. B.3.

the spot map based on the observed data. We have two major active longitudes where the area evolves in time with a period P=2.25 d and which is interpreted as a Rieger cycle.

A GLS periodogram of Test 2 time series recovers the main frequency ω_1 as well as the additional frequencies $(\omega_1 + \omega_2)$ and $(\omega_1 - \omega_2 = \omega_4)$ thus accounting for the observed periodicity $P_4 = 0.443$ d and indicating the Rieger cycle hypothesis as a plausible one. We note that the frequency $\omega_1 + \omega_2$ is hidden in the power background noise and becomes clearly visible only when the added Gaussian noise is removed. Therefore, we can account for its lack in the periodogram of the TESS time series.

Appendix C: Effects of rapid rotation and magnetic fields on Rossby waves

The perturbation of the frequencies of Rossby waves given by Eq. (5) under the effect of stellar rotation was analysed by Provost et al. (1981) and can be written as

$$\sigma \simeq \sigma_0 \left[1 + \left(\frac{\Omega}{\Omega_g}\right)^2\right], \tag{C.1}$$

where σ is the perturbed frequency, σ_0 the unperturbed frequency as given by Eq. (5), Ω the rotation frequency of the star, $\Omega_g = \sqrt{GM/R^3}$, σ_1 a coefficient depending on the wavenumbers m and n of the mode and the stratification of the density inside the star, G the gravitation constant, M the mass, and R the radius of the star (cf. Eq. 59 of Zaqarashvili et al. 2021).

We adopt a mass of our star of $M = 0.4\,M_\odot$ and a solar chemical composition (Z=0.02). A non-rotating stellar interior model has been computed using the Modules for Experiments in Stellar Astrophysics (MESA, see Paxton et al. 2019, and references therein) assuming a ratio of the mixing length to the pressure scale height $\alpha_{\rm mlt} = 2$ and their standard network of nuclear reactions. The radius of the star once it settles on the MS is found to be $R = 0.35\,R_\odot$, while the radius at the base of its convection zone is $r_b = 0.18\,R_\odot$.

Considering a mass $M = 0.4\,M_\odot$, $R = 0.35\,R_\odot$, and a convective stratification in the layer where the wave is propagating, we find a perturbation of the frequency of the wave of $\sim 23\%$ with respect to the value given by Eq. (5) for the considered mode with $n = 3, m = 1$. This is too a large value to be compatible with the observational error. On the other hand, assuming that the wave is propagating at the base of the convection zone at $r = r_b$, we get a perturbation of 3%, while, by assuming propagation on top of the radiative zone, we find a perturbation of only 0.1%. Therefore, the analysis of the rotational perturbation suggests that the Rossby wave assumed to be responsible for the P_2 periodicity is likely propagating close to the base of the convection zone or to the top of the radiative interior.

The presence of a strong magnetic field modifies the Rossby waves by splitting the unperturbed waves into two modes with higher and lower frequencies, respectively (cf. Sect. 3.3 of Zaqarashvili et al. 2021). We focus on the so-called fast magnetic Rossby waves as given by Eq. (76) of Zaqarashvili et al. (2021) because the frequency of the slow mode is much smaller than the rotation frequency in our case (cf. Eq. 77 of Zaqarashvili et al. 2021). Adopting the density given by our MESA interior model for the base of the convection zone ($\rho = 30.9\,\mathrm{g\,cm^{-3}}$) and a toroidal magnetic field of 10^5 Gauss, we find a relative perturbation of the frequency of the fast mode of 0.0021%, that is, completely negligible, because of the large predominance of the Coriolis force in our rapidly rotating star over the Lorentz force. For completeness, we estimate the frequency of the slow mode that is found to be 2×10^{-5} of the rotation frequency, that is, completely away from the range of the observed periodicities in our star. The perturbations of the Rossby wave frequencies scale with the square of the magnetic field intensity, therefore, the above conclusions are true also for magnetic fields stronger by more than one order of magnitude than the assumed field.